-RESEARCH PAPER-

International Journal of Mining and Geo-Engineering

IJMGE

IJMGE 58-2 (2024) 121-134

DOI: 10.22059/IJMGE.2023.363558.595090

Joint Euler deconvolution for depth estimation of potential field magnetic and gravity data

Saeed Ghanbarifar [a], Seyed Hossein Hosseini [a], Seyed Masoud Ghiasi [a], Maysam Abedi [b, *] and Ahmad Afshar [c]

[a] *Institute of Geophysics, University of Tehran, Iran.*

[b] *School of Mining Engineering, Faculty of Engineering, University of Tehran, Iran.*

[c] *Department of Mining and Metallurgical Engineering, Amirkabir University of Technology, Tehran, Iran.*

Article History:

Received: 08 August 2023.

Revised: 02 September 2023.

Accepted: 10 September 2023.

ABSTRACT

The Euler deconvolution system is a well-known approach to estimate the depth of underground sources in potential field geophysics. Over-determined Euler linear equations are usually solved independently and separately for the gravity and magnetic data, and each result is an estimate for the depth of the potential sources. This technique is widely utilized to analyze the depth variations of magnetic and gravity sources individually. However, the depth estimation of each of the mentioned potential fields may return specific and exclusive results regarding the complex nature of the subsurface structures, and the gravity and magnetic separate depth estimation solutions may be discordant in many aspects. In the cases of low-resolution for the gravity and magnetic data sets, this study indicates that the independently solved Euler depth estimation systems cannot yield reliable and accurate solutions for potential field sources. By combining the gravity and magnetic data and simultaneously solving the Euler equations for the gravity and magnetic potential fields, this research presents a novel approach called the joint Euler method with a proper capability to return more accurate and improved depth estimations for the boundary and body of potential field sources. The presented method was solved and examined over homogeneous and non-homogeneous synthetic scenarios with reduced resolution, and the depth solutions were also compared with the separate approach. After obtaining the desired results from the synthetic models, the joint Euler technique was applied to the gravity and magnetic data of the Kifl oil trap located in Iraq. The results were quite promising compared to the separate depth estimations, proving the sufficiency and applicability of the proposed potential field method in terms of interpretational aspects.

Keywords: *Joint Euler deconvolution, Euler depth estimation, Gravity and magnetic data sets, Kifl oil field.*

1. Introduction

As a popular and rapid strategy, the Euler equations have been vastly used in potential field geophysical studies to estimate depth of underground sources. Many efforts have been made to present uncomplicated and fast algorithms to quickly distinguish the geometry features of sought sources responsible for potential field anomalies, among which the Euler depth estimator is among the most favourite ones. Providing a basis for further in-depth researches, modelling and interpretations, a major advantage of this algorithm is its speed and simplicity. The standard Euler deconvolution method is extensively utilized in many researches for the interpretation of potential field geophysical data, since it carries less computational expense. Through potential field horizontal and vertical derivatives, the Euler equations are used to calculate the depth of subsurface sources reliably. To the best of our knowledge, over a profile of potential field data, this method was initially proposed and developed by Thompson (1982) [1]. Subsequently, Reid et al. (1990) solved the equations for 2D data [2]. Investigating the depth of mineral deposits, studying the location of potential field anomalies and shallow faults, calculating the depth of geothermal reservoirs, and also obtaining the thickness of surface sediments are some of the important applications of the Euler deconvolution method [3-5]. In addition to depth estimation, the Euler system of equations can also be used to determine the boundaries of anomalies and the depth of discontinuities, e.g. [6-7].

In previous studies, the standard 3D Euler equation system was solved for the data generated from potential sources by choosing an appropriate structural index “SI” within the optimum moving window sizes on the entire grid surface using the gravity and magnetic data sets separately and independently [8]. Due to the difference in the sensitivity of subsurface physical structures to different geophysical methods, as well as the existence of the principle of non-uniqueness, it may be necessary to use multiple geophysical methods throughout a study area in order to achieve and map more accurate and reliable results and viewpoints of underground features. Therefore, in the presence of the potential field gravity and magnetic data, this study presents a novel solution by introducing the "Joint Euler method", in which the standard Euler equations are solved simultaneously for both gravity and magnetic data. Then, this approach was tested on homogenous and non-homogenous synthetic cases.

* Corresponding author. *E-mail address:* : MaysamAbedi@ut.ac.ir (M.Abedi).

Assuming identical coordinates for magnetic and gravity potential data, the Euler equations were initially solved separately by reducing and eliminating the resolution of the potential field data. In this case, the results indicated that solving the Euler equations independently and separately does not return an accurate result for the boundary and depth of the survey potential sources. Due to various reasons, such as the high cost of geophysical surveys and the difficulty of the implementation, severe topography, etc., the resolution of magnetic and gravity data sets might be low in reality. In order to obtain more accurate results regarding the depth and boundary of potential sources for exploratory studies, tectonic researches, etc., geophysics and geological interpreters need access to novel methodologies to simplify data shortages. Therefore, the mentioned issue is fairly consequential and critical in the field of potential field data processing. In this regard, in the next step, the Euler equations are solved using the proposed joint Euler method with identical tolerance and inputs for the generated synthetic potential sources data with low-resolution.

To employ the presented approach on a real case, the Euler equations were solved in two separate and joint modes for the magnetic and gravity potential field data of the Kifl oil field in Iraq. Previous researches on this area confirm the existence of a long oil-trapping horst-graben fault structure [9-11]. The results indicate that solving the Joint Euler equations with the same initial tolerance and inputs yield better outcomes through proper agreement with geology and previous studies in comparison to the separately solved Euler solution of the equations.

2. Methodology

In this section, a brief introduction is presented to express the major mathematical concept of the proposed depth estimator. In the presence of a background field, the Euler's homogeneity equation for magnetic and gravity potential fields is written as follows:

$$(\mathrm{x}-x_0)\frac{\partial \mathrm{P}}{\partial \mathrm{x}}+(\mathrm{y}-y_0)\frac{\partial \mathrm{P}}{\partial \mathrm{y}}+(\mathrm{z}-z_0)\frac{\partial \mathrm{P}}{\partial \mathrm{z}}=\mathrm{N}(\mathrm{B}-\mathrm{P}) \quad (1)$$

Shortly describing the parameters, P stands for observed magnetic or gravity field data at a point (x, y, z); (∂P / x, ∂P / y, ∂P / z) describes the directional derivatives of the potential fields that can be calculated by different methods, such as convolution or calculation in the Fourier domain; (x_0, y_0, z_0) delineates the location of the anomaly source (z_0 is the depth of the potential field source); B is the background or main field of the observed data; and N stands for the structural index (SI) as the degree of homogeneity of the potential fields [12]. The structural index is normally variable for sources with different shapes, and its determination is very influential in the final depth estimates of the Euler system of equations [6-7]. Basic geological information of study areas has a great impact on obtaining this parameter. Various computational methods have been developed to calculate the structural index (e.g., [13-16]). Some important structural index values for homogeneous and simple-shaped geological structures are given in Table 1.

Rewriting the Eq. (1) separately for the magnetic field P_m and the gravity field P_g yields:

$$(\mathrm{x}-x_0)\frac{\partial \mathrm{P_m}}{\partial \mathrm{x}}+(\mathrm{y}-y_0)\frac{\partial \mathrm{P_m}}{\partial \mathrm{y}}+(\mathrm{z}-z_0)\frac{\partial \mathrm{P_m}}{\partial \mathrm{z}}=\mathrm{N_m}(\mathrm{B_m}-\mathrm{P_m}) \quad (2)$$

$$(\mathrm{x}-x_0)\frac{\partial \mathrm{P_m}}{\partial \mathrm{x}}+(\mathrm{y}-y_0)\frac{\partial \mathrm{P_m}}{\partial \mathrm{y}}+(\mathrm{z}-z_0)\frac{\partial \mathrm{P_m}}{\partial \mathrm{z}}=\mathrm{N_m}(\mathrm{B_m}-\mathrm{P_m}) \quad (3)$$

Indices of m and g denote the magnetic and gravity fields, respectively. Each of the above-mentioned equations has three common variables of source location ($\begin{bmatrix}x_0\\y_0\\z_0\end{bmatrix}$) and an independent unknown parameter of B ($\mathrm{B_g}$ for gravity and $\mathrm{B_m}$ for magnetic fields), which are obtained by solving Eqs. 2 and 3 independently. Adding $0\times \mathrm{B_g}$ to Eq. (2) and $0\times \mathrm{B_m}$ to Eq. (3), we have:

$$(\mathrm{x}-x_0)\frac{\partial \mathrm{P_m}}{\partial \mathrm{x}}+(\mathrm{y}-y_0)\frac{\partial \mathrm{P_m}}{\partial \mathrm{y}}+(\mathrm{z}-z_0)\frac{\partial \mathrm{P_m}}{\partial \mathrm{z}}+0\times \mathrm{B_g}=\mathrm{N_m}(\mathrm{B_m}-\mathrm{P_m}) \quad (4)$$

$$(\mathrm{x}-x_0)\frac{\partial \mathrm{P_g}}{\partial \mathrm{x}}+(\mathrm{y}-y_0)\frac{\partial \mathrm{P_g}}{\partial \mathrm{y}}+(\mathrm{z}-z_0)\frac{\partial \mathrm{P_g}}{\partial \mathrm{z}}+0\times \mathrm{B_m}=\mathrm{N_g}(\mathrm{B_g}-\mathrm{P_g}) \quad (5)$$

Combining the above-mentioned equations, it would be possible to simultaneously estimate the vector of unknown parameters $\begin{bmatrix}x_0\\y_0\\z_0\\\mathrm{B}_m\\\mathrm{B_g}\end{bmatrix}$. With (v + u) the number of observed data inside the window and for a window on the grid surface, the simple matrix form of the Euler equations (Eqs. 4 and 5) can be represented as follows:

$$\begin{bmatrix}\frac{\partial P_{m_1}}{\partial x_1} & \frac{\partial P_{m_1}}{\partial y_1} & \frac{\partial P_{m_1}}{\partial z_1} & N_m & 0\\ \vdots & & & & \\ \frac{\partial P_{m_u}}{\partial x_u} & \frac{\partial P_{m_u}}{\partial y_u} & \frac{\partial P_{m_u}}{\partial z_u} & N_m & 0\\ \vdots & & & & \\ \frac{\partial P_{g_1}}{\partial x_1} & \frac{\partial P_{g_1}}{\partial y_1} & \frac{\partial P_{g_1}}{\partial z_1} & 0 & N_g\\ \vdots & & & & \\ \frac{\partial P_{g_v}}{\partial x_v} & \frac{\partial P_{g_v}}{\partial y_v} & \frac{\partial P_{g_v}}{\partial z_v} & 0 & N_g\end{bmatrix}_{(v+u)\times 5} \times \begin{bmatrix}x_0\\y_0\\z_0\\B_m\\B_g\end{bmatrix}_{5\times 1} =$$

$$\begin{bmatrix}x_1\frac{\partial \mathrm{P_{m_1}}}{\partial x_1}+y_1\frac{\partial \mathrm{P_{m_1}}}{\partial y_1}+z_1\frac{\partial \mathrm{P_{m_1}}}{\partial z_1}+\mathrm{N_m}\mathrm{P_{m_1}}\\ \vdots \\ x_n\frac{\partial \mathrm{P_{m_u}}}{\partial x_u}+y_n\frac{\partial \mathrm{P_{m_u}}}{\partial y_u}+z_n\frac{\partial \mathrm{P_{m_u}}}{\partial z_u}+\mathrm{N_m}\mathrm{P_{m_u}}\\ \vdots \\ x_1\frac{\partial \mathrm{P_{g_1}}}{\partial x_1}+y_1\frac{\partial \mathrm{P_{g_1}}}{\partial y_1}+z_1\frac{\partial \mathrm{P_{g_1}}}{\partial z_1}+\mathrm{N_g}\mathrm{P_{g_1}}\\ \vdots \\ x_n\frac{\partial \mathrm{P_{g_v}}}{\partial x_v}+y_n\frac{\partial \mathrm{P_{g_v}}}{\partial y_v}+z_n\frac{\partial \mathrm{P_{g_v}}}{\partial z_v}+\mathrm{N_g}\mathrm{P_{g_v}}\end{bmatrix}_{(v+u)\times 1} \quad (6)$$

It should be noted that u and v stand for the number of the magnetic and gravity data in a single window, respectively.

The mentioned system of the equations can be written in the following simplified form:

$$\begin{bmatrix}\mathrm{G^m}\\\mathrm{G^g}\end{bmatrix}[\mathrm{m}]=\begin{bmatrix}\mathrm{d^m}\\\mathrm{d^g}\end{bmatrix} \quad (7)$$

Also, in a more simplified way, Eq. (7) can be represented as follows:

$$\mathrm{Gm}=\mathrm{d} \quad (8)$$

In this case, $\mathrm{d}=\begin{bmatrix}\mathrm{d^m}\\\mathrm{d^g}\end{bmatrix}$ is the data vector with the length of (v+u), m is the model parameters vector $\begin{bmatrix}x_0\\y_0\\z_0\\\mathrm{B}_m\\\mathrm{B_g}\end{bmatrix}$, and $\mathrm{G}=\begin{bmatrix}\mathrm{G^m}\\\mathrm{G^g}\end{bmatrix}$ is the linear operator in equations.

The set of matrix equations is an over-determined system for a window within the grid surface. The common method for finding the appropriate model parameters is to minimize the second norm of the residual vector, which is also known as the least squares technique. Due to the high ability in statistical analyses and having an appropriate geometric understanding, the least squares method, or also the second norm solution, is a popular approach in solving equations with a normal distribution. To increase the certainty of the answers, the least squares method is generally written in the form $\mathrm{G_w m}=\mathrm{d_w}$. In this case, the residual vector turns into the following form [17]:

$$\mathrm{r}=\mathrm{d_w}-\mathrm{G_w m} \quad (9)$$

In the above- mentioned formula, it is better noting that $\mathrm{d_w}=\mathrm{d}\times \mathrm{W}$ and $\mathrm{G_w}=\mathrm{G}\times \mathrm{W}$.

Table 1. The structural indices of some simple-shaped sources in potential field studies (Reid and Thurston 2014).

Source	Number of infinite dimensional	Magnetic	Gravity	Depth relative to...
Sphere	0	3	2	Center
Vertical line/pipe/cylinder	1	2	1	Top
Horizontal line /cylinder	1	2	1	Center
Dyke	2	1	0	Top
Sill	2	1	0	Center
Contact	3	0	-1	Top

This research considered the weighting function (W) as a diagonal matrix which is inversely related to the distance of the observed data (s) from the center of each window:

$$W=\begin{pmatrix} \begin{pmatrix} 1/s_1 & \cdots & 0 \\ \vdots & \ddots & \vdots \\ 0 & \cdots & 1/s_u \end{pmatrix} & \cdots & \begin{pmatrix} 0 & \cdots & 0 \\ \vdots & \ddots & \vdots \\ 0 & \cdots & 0 \end{pmatrix} \\ \vdots & \ddots & \vdots \\ \begin{pmatrix} 0 & \cdots & 0 \\ \vdots & \ddots & \vdots \\ 0 & \cdots & 0 \end{pmatrix} & \cdots & \begin{pmatrix} 1/s_1 & \cdots & 0 \\ \vdots & \ddots & \vdots \\ 0 & \cdots & 1/s_v \end{pmatrix} \end{pmatrix} \quad (10)$$

Considering the mentioned weighting function, the simple form of the Euler equations system turns into the following form:

$$G_w m = d_w \quad (11)$$

Multiplying both sides of Eq. (1) by the transposed matrix of G_w, we have:

$$G_w{}^T G_w m = G_w{}^T d_w \quad (12)$$

Finally, the normal form of the equations for obtaining the model parameters (m) is presented as follows [17]:

$$m = \left(G_w{}^T G_w\right)^{-1} G_w{}^T d_w \quad (13)$$

It should be noted that in this study, the dynamic window method has been utilized to solve the Euler equations in each part of the grid surface [8]. This method solves the Euler equations for potential fields by considering moving and dynamic windows throughout the whole grid surface. By considering dynamic windows with variable dimensions in each area of the grid, this algorithm solves the Euler equations within all the windows, and finally, the window with the minimum uncertainty value in depth estimation is considered the optimal one. The entire grid surface is scanned and the optimal window sizes are calculated along with minimum error rates for answers and dimensions simultaneously. Finally for the entire observation grid, the set of acceptable answers for the Euler equations is the ones with an uncertainty of less than an initial tolerance (ε) that is also a percentage of the estimated depth. Briefly stated, the set of acceptable answers to the Euler equations can be obtained from the following conditional expression [8]:

$$\text{if } \min(\text{uncertainty}_k)(i,j) < \varepsilon \left(\frac{z_0}{100}\right) \Rightarrow \text{final } m_{\text{euler}} \text{ estimation} \quad (14)$$

Note :$0 < \varepsilon < 100$

3. Synthetic scenarios

In this section, to evaluate the efficiency of the proposed method, the joint Euler method was examined and reviewed for two synthetic models. Since the Euler deconvolution technique concerns homogenous sources, this method was initially tested for a homogenous sphere, and then it was utilized over a more complicated inhomogeneous synthetic body.

In this regard, the survey resolution of the gravity and magnetic data was reduced for the inhomogeneous synthetic data, and then the Euler equation system was solved independently and jointly for the gravity and magnetic potential fields to evaluate the impact of the presented joint solution on solving the Euler equations. In this research, the synthetic magnetic and gravity survey coordinates are investigated at two identical and non-identical states for an inhomogeneous source, and the results are reviewed and discussed.

To simulate the responses of the synthetic magnetic and gravity models, a grid area was designed .Using the parallel algorithm in Matlab through cell merging method, Chen and Zhang (2018) developed a forward modelling code on gravity data [18]. Building upon this work, both magnetic and gravity data were forward modeled. To create more realistic terms, the magnetic and gravity data were corrupted with 3 % and 1 % random Gaussian noise, respectively. These observations are then inputs and entries of the aforementioned Euler equations system.

3.1. Homogenous model

To test the presented synthetic method, a simple homogeneous sphere source was initially considered. The magnetic susceptibility and density contrast properties of this model were 0.1 (in SI unit) and 0.3 (gr/cm^3), respectively. The Earth's magnetic field intensity of 46,000 nT with inclination and declination angles of 90 and 0 degrees, respectively, were assumed. As can be seen in Fig. 1, the magnetic and gravity field responses are presented within a surface grid covering a 1000*1000 m^2 area with a 10 m station spacing along with a 3D view of the synthetic model and a 2D top view of the source. A summary description of the first synthetic scenario is given in the Table 2.

The potential field of a homogeneous source was calculated with the coordinates of the center (x_c, y_c, z_c) = (500, 500, -100) and a radius of 50 meters. Then, the depth estimation process was conducted using the presented joint standard Euler deconvolution method with dynamic windows ranging from a minimum of 3 times cell size to maximum of 33 times cell size, by considering 1% tolerance and 90% overlap. In the next step, the obtained results with the real values (center of the sphere) were compared. The results of the histogram of the estimated parameters (Fig. 2) indicate that most of the depth solutions (z_0) are obtained between the values of 100.95 and 101 meters around the location (x_0, y_0) of 500 meters, in close accordance with the assumed values.

Now, if we consider the average value of the parameters as the criterion for comparing the answers with the real center of the sphere at the coordinates (x_c, y_c, z_c) =(500,500,-100), the obtained average values and errors indicate that the presented joint Euler method has appropriately estimated the coordinates of the center of the homogeneous sphere (tabulated in Table 3).

3.2. In-homogenous model

Using the mentioned forward-modelling technique, to test the presented method, a synthetic model with two separate sources was planned. The western source was initially considered with a depth range of 200-500 m and a NS elongation from 1900 to 3000 m, and also an EW elongation from 1300 to 1900 m. The magnetic susceptibility and density contrast properties of this model were 0.01 (in SI unit) and 0.5 (gr/cm^3), respectively.

The eastern source was also specified with a depth range of 300-600 m and a NS elongation from 1900 to 3000 m, and also an EW elongation from 3500 to 4100 m. The magnetic susceptibility and density contrast properties of this model were 0. 1 (in SI unit) and 1 (gr/cm^3), respectively.

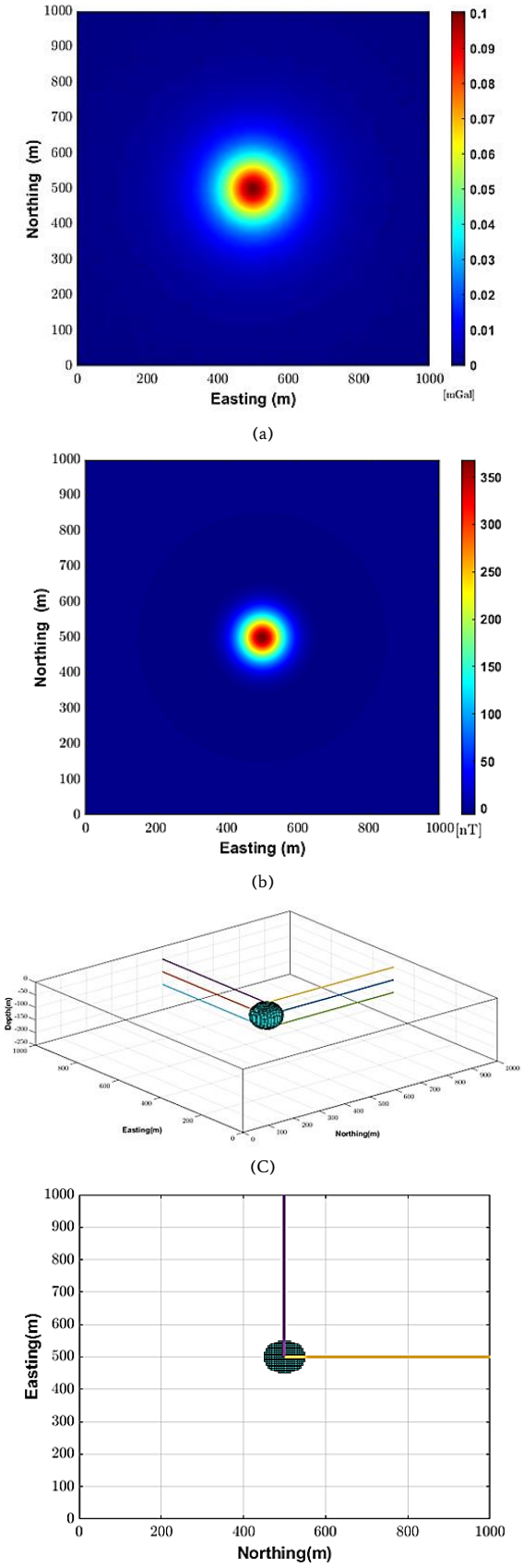

Fig. 1 A homogeneous sphere source potential field anomaly simulation, (a) gravity data, (b) magnetic data, (c) 3D source geometry, and (d) 2D top view. The synthetic gravity and magnetic data are corrupted by1% and 3% random Gaussian noise, respectively.

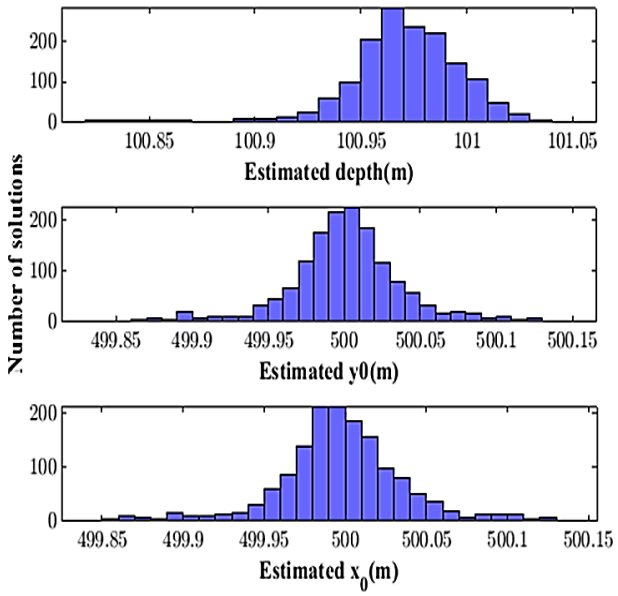

Fig. 2 The histogram plot of the estimated parameters (x0, y0, z0) through the joint Euler algorithm. A synthetic sphere source was assumed as described in Table 2.

The Earth's magnetic inclination and declination angles were assigned equal to 90 and 0 degrees, respectively and also the Earth's main field for the magnetic source was also considered equal to 46,000 nT. A summary description of the synthetic scenario is delineated in Table 4. As can be seen in Fig. 3, the magnetic and gravity field responses of the two horizontal sources are presented within a surface grid covering a 5000*5000 m^2 area with a 50 m station spacing along with a 3D view of the synthetic model and a 2D cross section indicating the middle of the area.

In standard Euler deconvolution method, structural index (SI) is the coefficient delineating the geometric characteristics of causative sources responsible for potential field anomalies. Depth estimation is highly dependent on the structural index [19], while it can be estimated automatically by manipulating the main equation of Euler and substituting input data with directional derivatives of potential field data [14]. For the designed synthetic model, it should be noted that the Euler standard equations are solved with a structure index of 1.5 and 0.5 for magnetic and gravity fields, respectively ($N_g = N_m$-1).

In the following, the Joint Euler depth estimation approach is compared with the separately solved examples for four different cases.

3.2.1. CASE 1: non-identical magnetic and gravity coordinates

In this case, the observed magnetic and gravity survey coordinates are assumed to be non-identical. As depicted in Fig. 4, the number of potential magnetic and gravity data was reduced so that the remaining data of the gravity and magnetic potential fields do not have the same coordinates. In this way, by reducing the resolution of magnetic (or gravity) data, some gravity data points may exist at the missing magnetic data locations. Data-spacing is also increased from 50 m to 150 m. White squares indicate the lack of survey data. The Euler equation system was then solved separately for each of the magnetic and gravity data sets. As shown in Fig. 3, the results of the simulations show that separate estimation of the depth of the potential sources results in deficient resolution, while increasing the survey data distances.

Figure 5 indicates the results of the standard Euler depth estimation technique for each of the magnetic and gravity data after reducing the survey data resolution. As mentioned before, due to the deficiency of the data resolution, the standard Euler depth estimation process was not able to retrieve any depth solutions either for magnetic or for gravity data (Fig.5).

Table 2. The assumed parameters for the synthetic homogeneous source shown in Fig. 1.

Easting Center (m)	Northing Center (m)	Z Center (m)	Radius (m)	Density contrast (g/cm³)	Susceptibility (SI)	Inclination (degree)	Declination (degree)
500	500	-100	50	0.3	0.1	90	0

Table 3. The average values of the estimated parameters for the center of the homogeneous sphere using the joint Euler method.

Parameters	x_0	y_0	z_0
Average estimated parameters for magnetic sphere	499.9975	500.001	100.9698
Error	0.0049495	0.0020678	0.9698

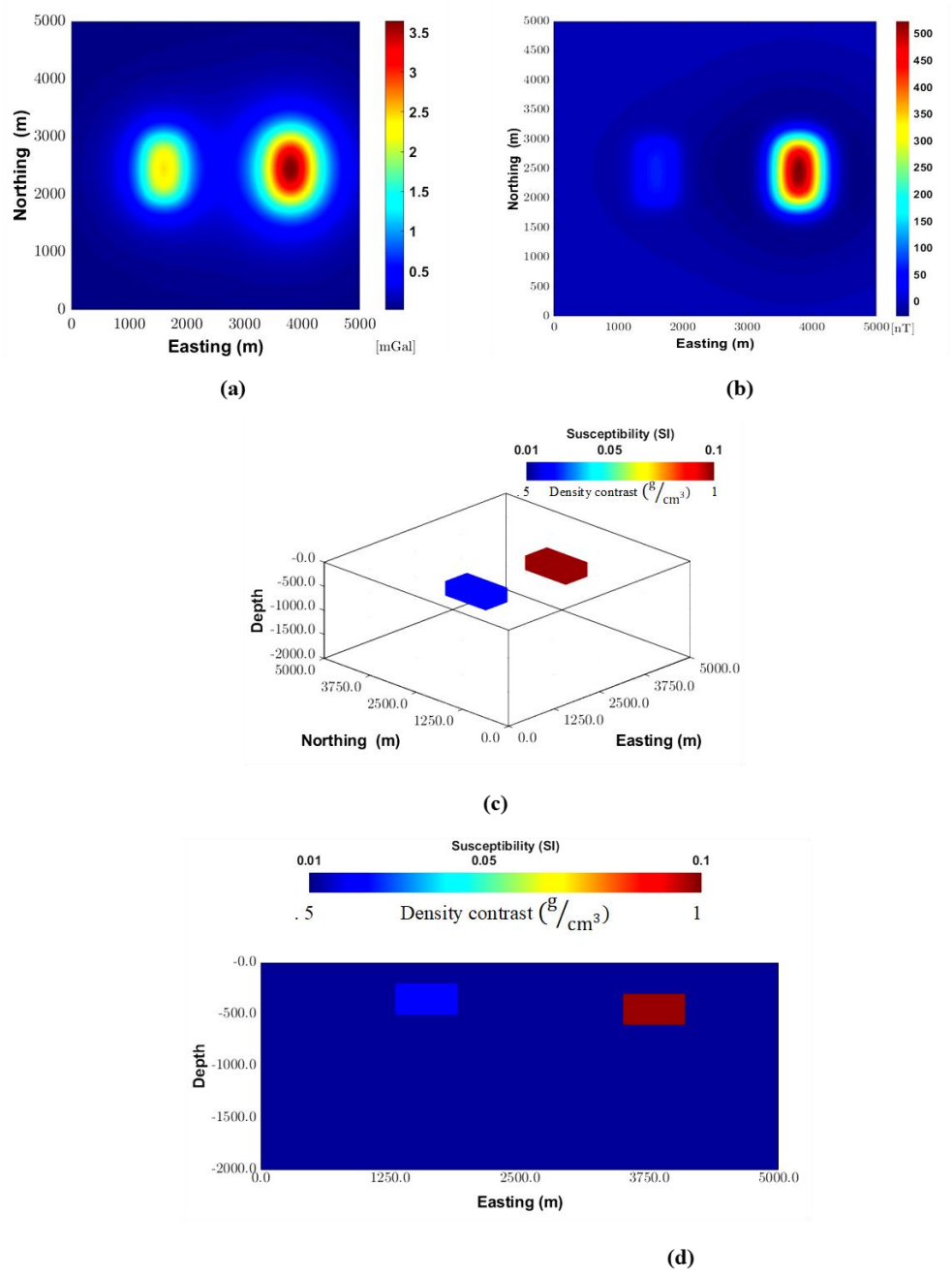

Fig. 3 The potential field anomaly simulation of a multi-source scenario with 50 m spacing, (a) gravity data, (b) magnetic data, (c) 3D view of sources geometry, and (d) 2D cross section at Northing=2500 m. The synthetic gravity and magnetic data are corrupted by 1% and 3% random Gaussian noise, respectively.

Table 4. The assumed parameters for the synthetic model shown in Fig. 3.

West Block Size (m)	Easting (m)		Northing (m)		Z (m)		Slope (degree)	Density contrast (g/cm3)	Susceptibility (SI)	Inclination (degree)	Declination (degree)
	From	To	From	To	From	To					
600 1100 300	1300	1900	1900	3000	-200	-500	-	0.5	0.01	90	0
East Block Size (m)	**Easting (m)**		**Northing (m)**		**Z (m)**		**Slope (degree)**	**Density contrast (g/cm3)**	**Susceptibility (SI)**	**Inclination (degree)**	**Declination (degree)**
	From	To	From	To	From	To					
600 1100 300	3500	4100	1900	3000	-300 -600		-	1	0.1	90	0

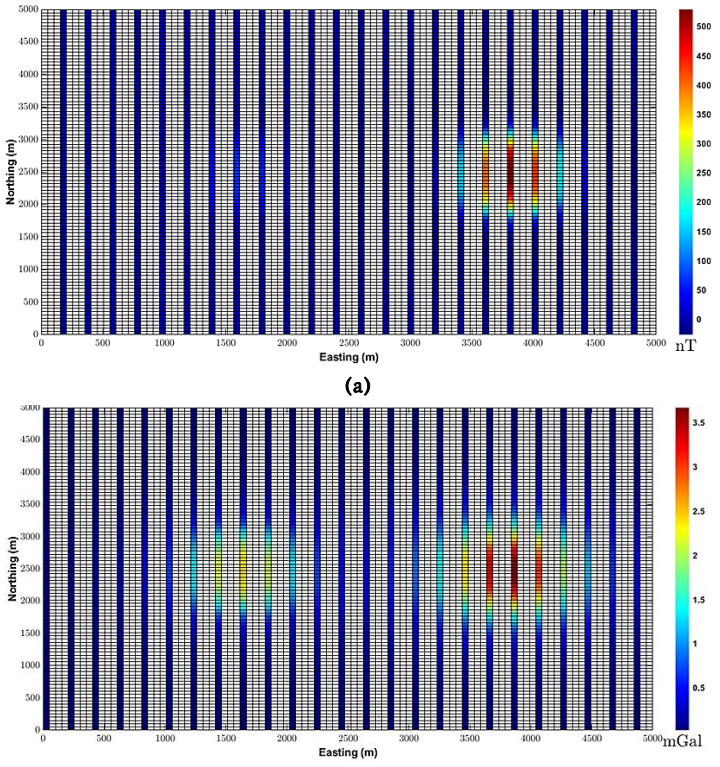

Fig. 4 The observed synthetic anomalies for the simulated potential fields of a multi-source scenario, (a) magnetic data, and (b) gravity data. Note that white squares indicate the lack of data as a result of resolution reduction.

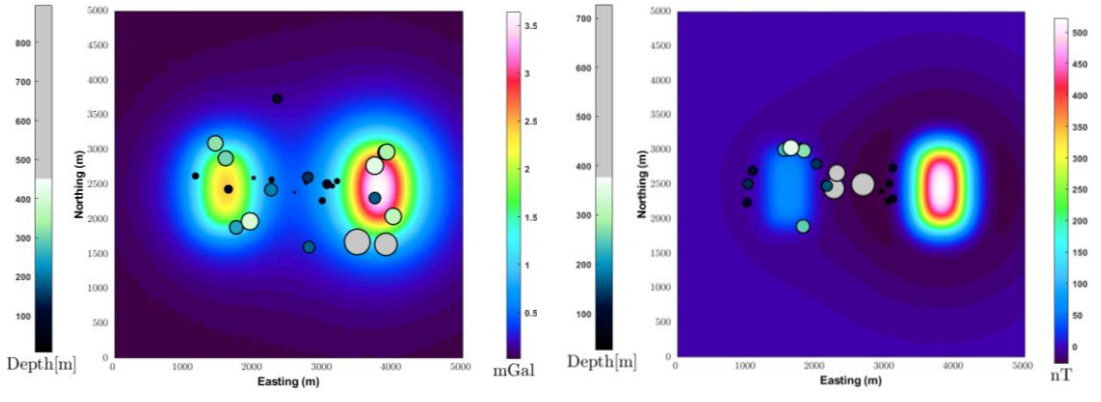

Fig. 5 The standard Euler depth estimation of a multi-source scenario, where the left column is for gravity and the right one is for magnetic data. Data resolution has decreased.

To address the mentioned issue, the proposed solution of this study is to utilize the joint Euler approach which solves the equations considering both of the potential fields simultaneously. For this purpose, in order for better visualization, the gravity and magnetic survey profiles are shown concurrently in Fig.6a. As can be seen, it is assumed that a number of important survey magnetic data points are unavailable. Therefore, by the available gravity data in some of these points, the Euler equations can be jointly solved using the proposed solution of this study. The results of the joint Euler solutions with two different tolerance values of 3 and 5 are shown in Fig. 6.

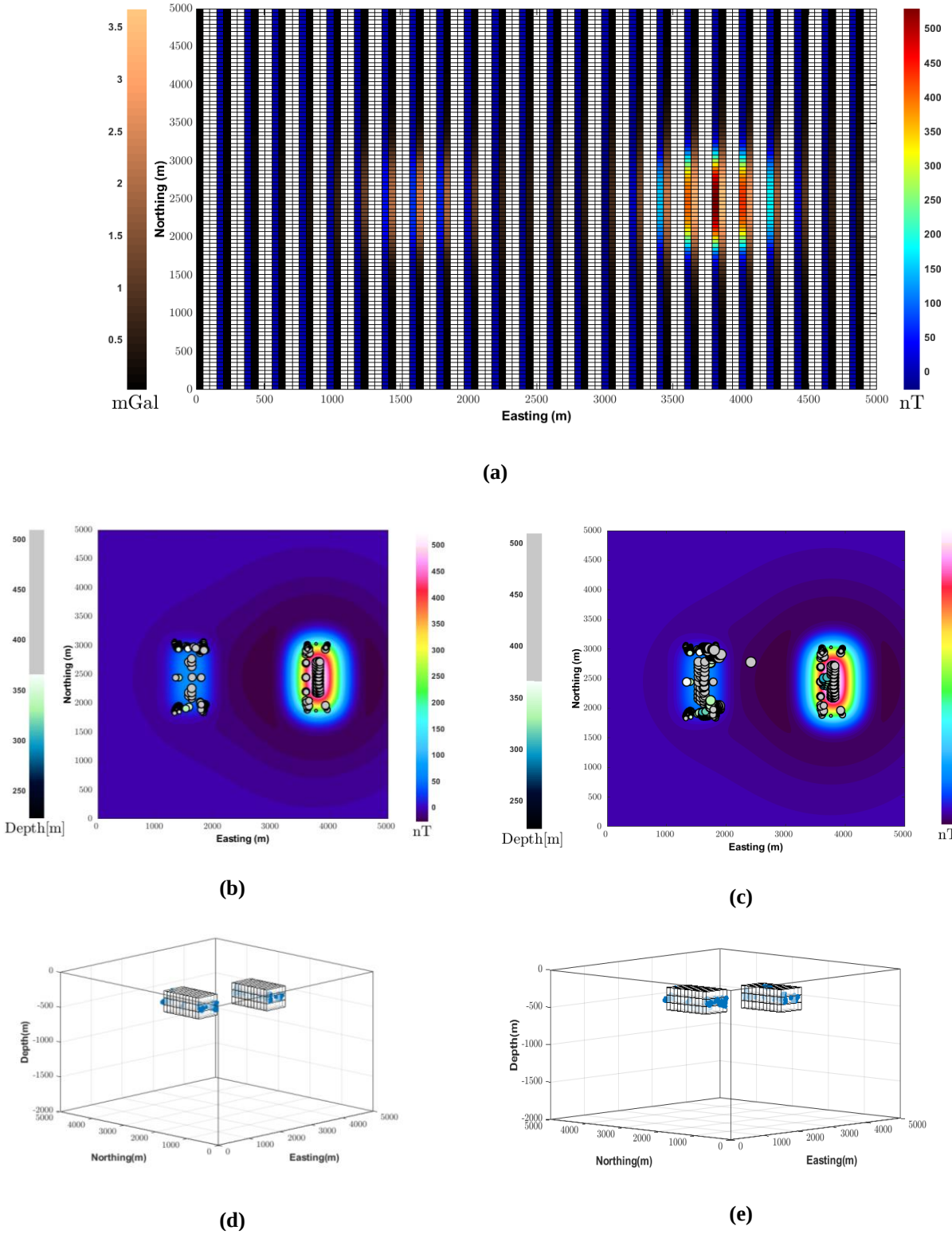

Fig. 6 (a) The observed gravity and magnetic data of a multi-source scenario superimposed on the same map and joint Euler depth estimations for synthetic sources with tolerance of (b) ε=3 and (c) ε=5. The 3D transparent display of depth estimations for tolerances of (d) ε=3 and (e) for ε=5.

As can be inferred from Fig. 6, comparing the results with the initial synthetic model (Fig. 3), despite the relatively lower resolution, it can be concluded that the joint Euler method was able to provide an appropriate estimation of the depth and location for two potential sources. By considering the complex geological, morphological, and topographic features of the Earth, in practice, this method decreases the uncertainty in the absence of some of the magnetic or gravity data points. This presented approach is also very useful for datasets with lower resolutions and quality. It should be mentioned that the joint Euler depth estimation results are illustrated on the magnetic map in Figs. 6b and 6c, and accordingly, enlarging the tolerance caused a minor increase in the number of solutions. The joint Euler solutions superimposed on Figs. 6d and 6e also display the 3D transparent view of the synthetic forward models. As can be observed, the joint Euler depth solutions are acceptably located over the causative sources.

3.2.2. CASE 2: Identical magnetic and gravity survey coordinates

Similar to Fig. 4a, in this section, the resolution of magnetic survey data is assumed to be relatively low, while the gravity survey data are available at the same magnetic data points. In this case, as indicated previously, solving the Euler equations system independently for the magnetic and gravity data sets does not lead to an accurate estimation of the depth and boundaries of the potential sources (Fig. 7). Therefore, the Euler equations were solved simultaneously for both of the magnetic and gravity potential fields by considering two tolerances of 3 and 5. Briefly stated, the Joint Euler solution approach contributes to the reduction of the possible lack of resolution and presents a much more precise depth estimation process (Fig. 7c). The results show that Joint Euler technique has been quite able to estimate the depth and boundaries of potential sources with the lack of magnetic data resolution.

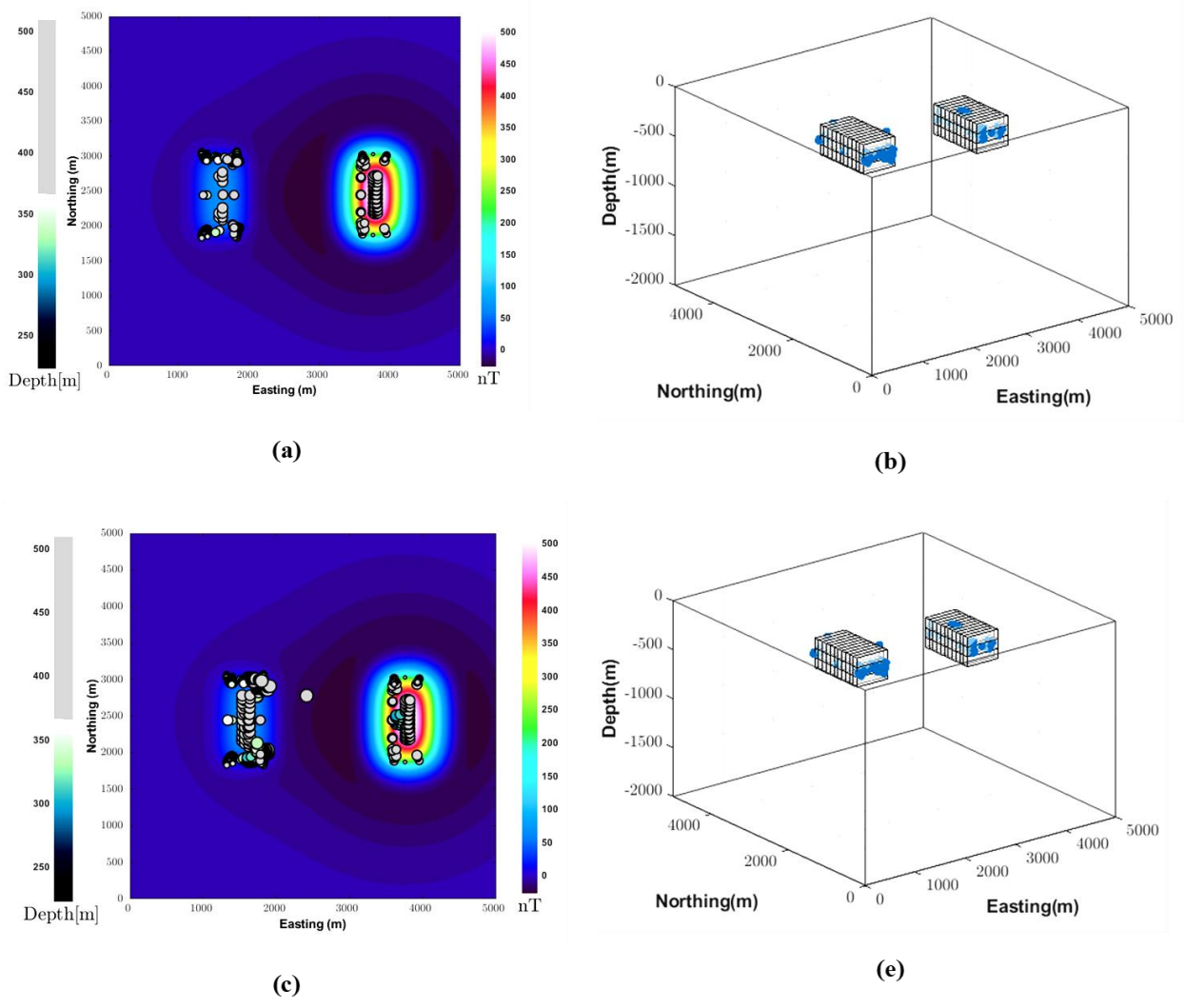

Fig. 7 The joint Euler depth estimation of a multi-source scenario, (a) depth solution plot on the magnetic anomaly for ε=3, (b) The 3D transparency display of the source and solutions for ε=3, (c) depth solution plot on the magnetic anomaly for ε=5, and (d) The 3D display of the source and solutions for ε=5.

As discussed through synthetic tests in this section, the impact of the joint Euler depth estimation approach was specifically indicated when the magnetic and gravity survey data resolution is relatively low. Comparing the results with the initial synthetic models, in cases with the lack of precision through separate magnetic and gravity depth estimation solution, the joint Euler attitude was synthetically proven to be quite applicable.

3.2.3. CASE 3: Generating responses with increase of data-spacing

To examine the joint Euler method in this section and to create a realistic condition for the synthetic experiments, the data spacing interval was increased from 50 m to 208 m, calculating the synthetic magnetic and gravity responses of the same multi-source scenario. The Euler equations system was then solved by considering a 5 % tolerance for the estimated depth ranges. Similar to the previous hypotheses, it

should be noted that the synthetic survey coordinates were identical for both data sets.

Figure 8 depicts the Euler depth solutions for the gravity and magnetic data along with the joint approach results. As can be seen, increasing the data spacing caused a major decrease in the number and precision of the solutions for the gravity and magnetic separate Euler depth estimations. As can be inferred from Figs. 8a and 8b, the single gravity and magnetic depth estimations did not lead to a proper trustworthy conclusion which can be an acceptable criterion for further investigations and drilling operations. As in the magnetic results in Fig. 8b, the gravity depth estimation shown in Fig. 8a could not retrieve a sustainable estimate for the depth and location of the potential field sources, but this fact is more evident for the western source, which has a lower geophysical signal amplitude than the eastern one. However, due to the existence of adjacent anomalies, it would be more difficult to set up a suitable window size for solving the Euler equations, because it is not possible to overlap the windows on one side from one place to another.

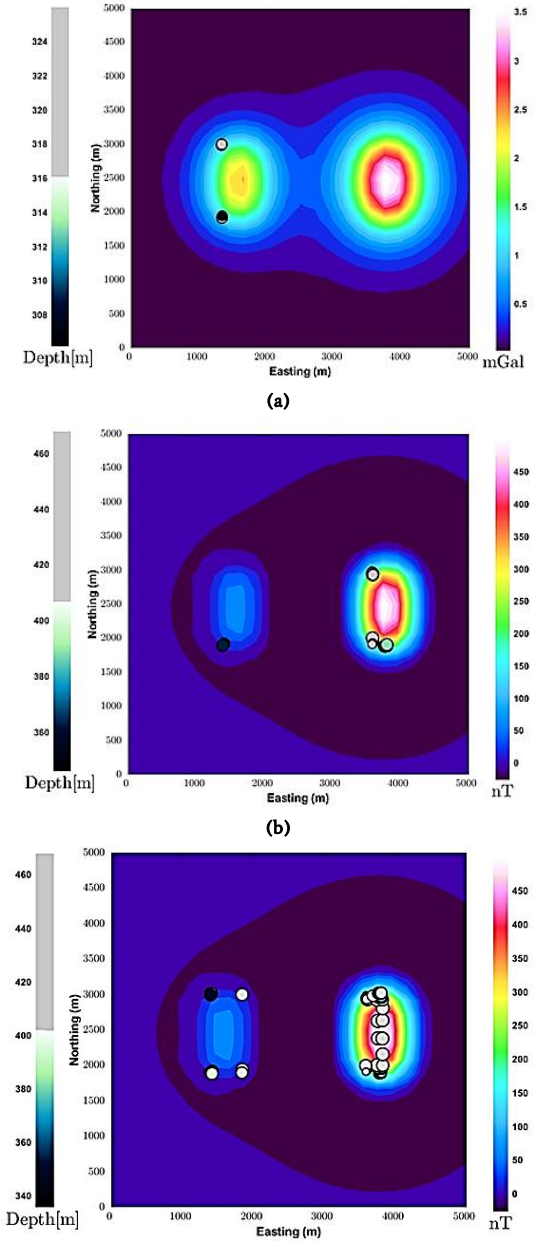

Fig. 8 (a) The Euler deconvolution depth estimation for separate (a) gravity data, and (b) magnetic data, and (c) joint algorithm for both potential fields.

In the next step, as depicted in Figs. 8c, the presented joint procedure of this research was conducted over the same synthetic data with the same tolerance value. In this case, the number and clustering of the retrieved depth solutions increased significantly for both the eastern and western potential sources simultaneously. Compared to the results in Figs. 8a and 8b, the retrieved depth estimation points are fairly distributed over both sources, especially for the eastern mass which was not properly determined through the common Euler equations of the gravity synthetic data set. For the western source, the estimates were also quite pleasing in terms of the number of the solutions compared to the separate estimation conclusions for the potential sources. This experiment proves the validity of the proposed joint method, specifically where the separate magnetic and gravity depth estimations fail to recover acceptable results. Reducing the potential field data resolution is an appropriate technique to test the effectiveness and sustainability of the joint procedure.

It should be mentioned that increasing the tolerance can lead to an increase in the number of estimated points, but it also increases the error in the estimation of parameters at the same time. Reducing the tolerance may also cause the loss of some of the beneficial estimations. Therefore, this research seeks to obtain the parameters through pre-determines error in this section. This behavior may even occur for different tolerances in high-resolution states.

3.2.4. CASE 4: Non-identical coordinates with increased data-spacing

In this section, the survey data spacing was increased to 192 and 384 meters for the magnetic and gravity data, respectively, resulting in different data coordinates for both potential field data points. Then, the Euler equations were solved separately and jointly with the same inputs and a 5% tolerance for these data. The depth estimation outputs for the gravity and magnetic data are presented in Fig. 9.

As can be seen in Fig. 9a, compared to the previous step, reducing the resolution of the gravity data, it is evident in this case that the algorithm returns no result from solving the Euler equations within the determined tolerance interval (5%). Although the magnetic results from solving the equations yielded better estimations from the gravity solutions, comparing the number of the solution points on the eastern mass (Figs. 9b and 9c) indicates that in comparison to the Joint Euler mode, the number of these acceptable solutions is substantially less, and the proposed Joint Euler approach has been successfully able to estimate the depth over the body and its boundaries .Therefore, despite the very small number of gravity data (low-resolution) and the lack of acceptable Euler depth estimation results for the gravity data with low-resolution, the same number of data points has been quite helpful to improve the results of the joint Euler approach. These results also prove that the proposed joint Euler method has been able to enhance the results of depth estimations in this case as well.

It should be mentioned that in the following, the Euler equations for the real magnetic data were able to determine the boundaries of the faults, while the gravity results were not useful on one of the zones with depth solutions. However, the results of the joint Euler were able to retrieve the depth of the sedimentary layer in addition to the boundaries of the faults.

4. Geological setting of the studied region

The Iraqi geology is tectonically divided into four main zones with the different characteristics of rock type, age, thickness and structural evolution. As can be seen in Fig. 10, these major zones include: (1) Inner Platform (stable shelf), (2) Outer Platform (unstable shelf), (3) Shalair Zone (Terrain), and (4) Zagros Suture Zone. The first two zones of the Arabian Plate have not been subjected to any kind of metamorphism and volcanism. The Iraqi territory is located in the extreme northeastern part of the Arabian Plate, which is colliding with the Iranian (Eurasian) Plate. This collision has developed a foreland basin that includes: (1) Imbricate Zone, (2) High Folded Zone, (3) Low Folded Zone, and (4) Mesopotamia Foredeep [20].

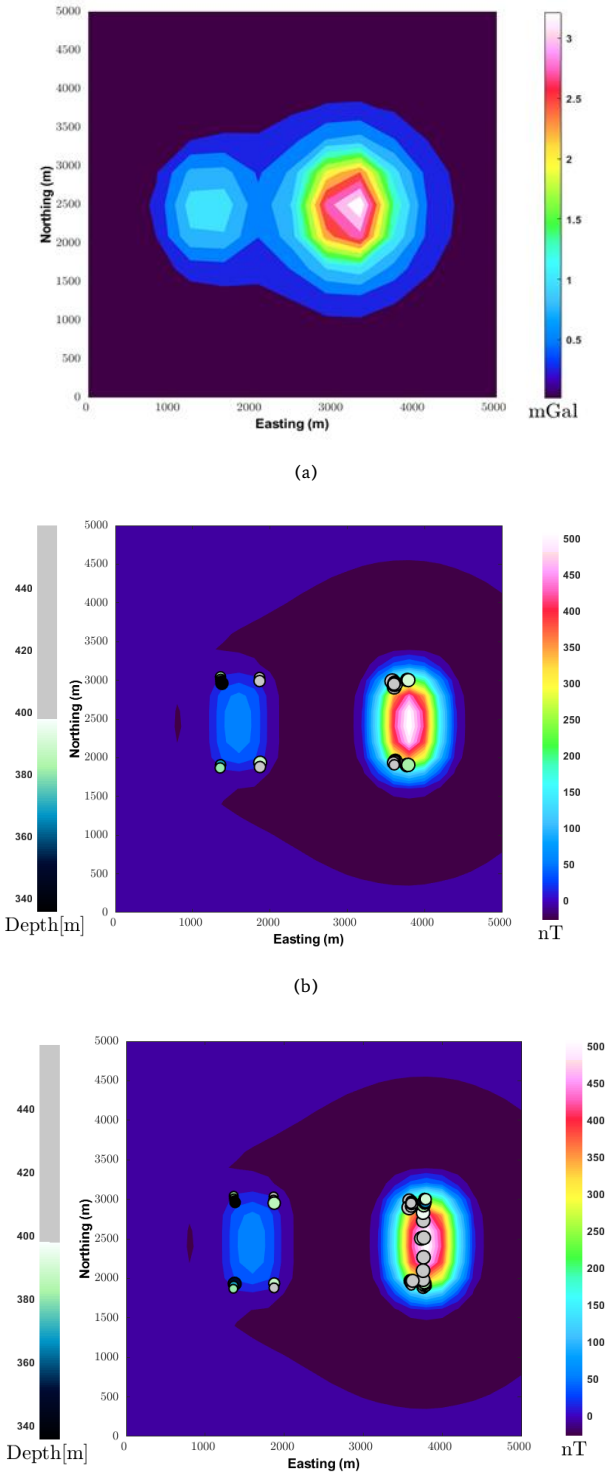

Fig. 9 (a) The Euler deconvolution depth estimation for separate (a) gravity data, and (b) magnetic data, and (c) joint algorithm for both potential fields.

The Mesopotamia foredeep in Iraq includes the Mesopotamia Plain and the Jazira Plain. Compared to the Imbricate, High Folded and Low Folded Zones, this foredeep is less tectonically disturbed. Known as the Mesopotamian Flood Plain, Quaternary alluvial sediments of the Tigris and Euphrates Rivers and their tributaries as well as distributaries cover the central and southeastern parts of the Foredeep entirely. However, covered by Miocene rocks, the extension of the Mesopotamia Plain towards the northwest is called the Jazira Plain, represented by a thick sedimentary sequence. The Mesopotamia Foredeep thickens northwestwards, including syn-rift sediments, especially of the Late Cretaceous age, whereas on the surface, the Quaternary sediments thicken southeastwards. The basement depth also varies from 8 km in the west to 14 km within the Iraqi–Iranian boarders towards the southeast. In the southern part of the Mesopotamia foredeep, the anticlinal structures have an N–S trend and extend northwards until the Latitude 32N. Within the Jazira Plain, they change their trends to NW–SE, and then to E–W direction [20-21].

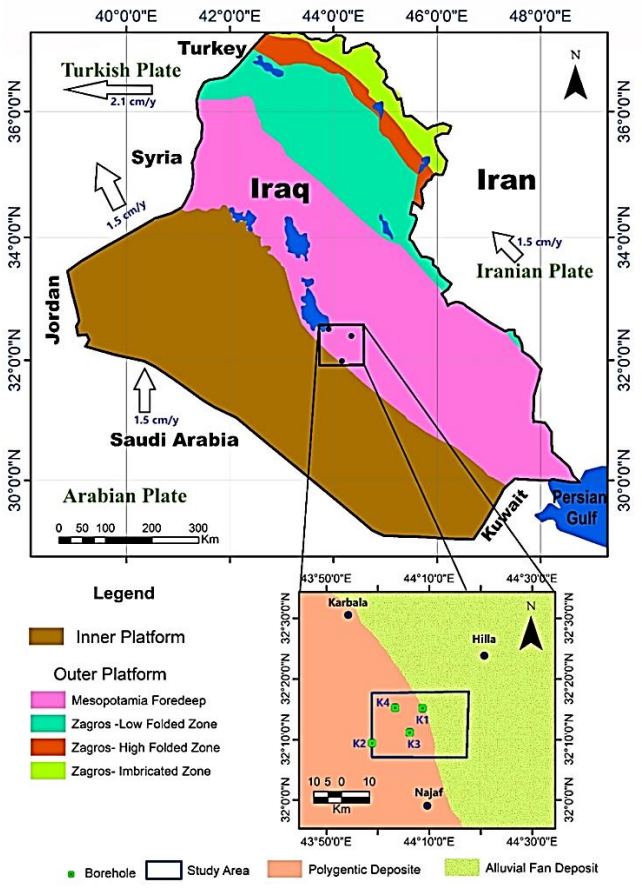

Fig. 10 The main Tectonic Zones in Iraq (arrows indicate plate motions in centimeters per year) and the studied oil field in the Kifl region.

The studied area is geographically located in the center of Iraq and west of the Euphrates River, about 30 km southwest of the city of Hilla and between the cities of Karbala and Najaf. This area is located between latitudes of 32° 08′ 08″- 32°17′ 03″ N and longitudes of 44° 07′ 50″- 44° 21′ 07″ E. In terms of tectonic settings, superficial sediments of the Kifl area range from the Eocene in the southwest to recent deposits on the Euphrates zone in the east. They often indicate a very slight dip towards the east and northeast (two degrees). The majority of the faulted area is also covered by Quaternary sediments [22-23]. As one of the most prominent Najd fault zones, the faults belong to the Euphrates boundary running toward the Euphrates River in the south of Iraq and continuing towards the Rutba area in the west [24]. Although, in adjacent areas, 49 minor normal faults have occurred with a general trend of NW-SE and N-S [25]. Generally, the study area is considered stable in terms of tectonics. In addition, the sedimentary cover ranges from 7-8 km overlying the basement rocks.

The Kifl area is positioned in the stable shelf within the Mesopotamian zone and in the Euphrates subzone. It represents the boundary between the stable and unstable shelf. The geological and tectonic evolution of Iraq is considerably influenced by the opening and

closing of the Palaeotethys and Neotethys oceans. The Neotethys was opened during the upper Carboniferous-Permian period along the rifting axis running parallel to the Zagros, and when the Arabian plate was dominated by post-rift thermal sag. It led to generating a passive margin to the northwest and northeast, which progressively prograded basin wards from W/SW to the E/NE. The new Tethys Ocean continued to spread to the NE, and the Mediterranean in the north began to open in the Late Jurassic. The Mesopotamian intercontinental basin developed inside the Arabian plate and to the west of the Zagros thrust zone. Consequently, the Kifl area was affected by those movements. It was located on the west flank of the Mesopotamian basin.

The transversal faults have played important roles in the depositional basin environment, and later in the development of the main tectonic structures. It means that the faults have been active since the Permian [26]. The main structural elements recognized and described up to now were mostly those caused, or at least to a different degree, directly affected by the Alpine Orogenic phases, mainly by the tertiary ones. Therefore, the trends of the subsurface features in this block are parallel to the Alpine chain, prevalently NW-SE and N-S. The geological background of the area was affected by the geometry of the underground basement masses and faults. Moreover, it is also affected by the Paleozoic epirogenic events and Mesozoic arching [22].

In 1959, the K1 exploration well was drilled on the crest of this structure, which penetrates the mid Jurassic-Triassic formations. The drilling reaches 3256.5 m at the Sargelue formation, approving oil-trapping in the Nahr Umar and Zubair formations. The estimated production is approximately 5600 b/d. Then, the K2 well was drilled 13.5 km southwest of the K1, without indicating oil-trapping since it lay outside the structure enclosure of the field. Both K1, K2 were localized through the interpretation of gravity and seismic surveys executed by the IPC company in late 1950s. Based on the results of a seismic survey in 1975, the K3 well was drilled to explore the Triassic reservoir and to evaluate the amount of hydrocarbon accumulations appeared at the K1 well. The drilling reached a depth of 4330 m at the Kura chine formation. According to the log interpretations, the oil indicator was 1.5 m higher in the Zubair formation. In 1980 and 1982, the Mobil Company studied the area and attributed the presence of oil in the Zubair formation due to stratigraphic traps. Therefore, the K4 well was drilled, located 4 km west of the K1 to ensure obtaining the longest oil column within the sand body. However, the results proved that the Zubair formation is structurally thick by about 10 m in the K4 relative to the K1, while oil column in the K4 was 3 m. Note that the K4 well was drilled for the estimation of hydrocarbon accumulation in the Zubair and the Yamama formations, and to understand how the oil was trapped.

5. Case study geophysics survey and data interpretation

In this section, the Euler equations were solved and compared in both separate and joint modes for the real magnetic and gravity data of an oil-trapping field in the Kifl, Iraq, and the results are discussed. For this purpose, a grid of the surveyed data in the area with a spacing of 200 m^2 and the dimensions of 2,000 * 1,200 m^2 was prepared. The reduced to pole map of the magnetic residual data and the Bouguer anomaly map are depicted in Fig. 11. It shall be mentioned that the residual anomaly maps lead the way to specify the most important local features of the Kifl area and obtain a suitable geometry of different underground structures. The investigation of the gravity and magnetic potential fields as well as previous studies in the area indicate the existence of a hidden fault in the form of horst and graben structures along with an oil trap in the region [11].

Figures 12 to 14 illustrate the depth estimation results of the standard Euler equations in 2D and 3D visualization for the potential field maps. Due to the existence of the subsurface two-dimensional structures in the area, and according to the basic geological information, also previous studies in the region, the structural indices of 1.5 and 0.5 were considered, respectively for the magnetic and gravity data for solving the equations [9-11].

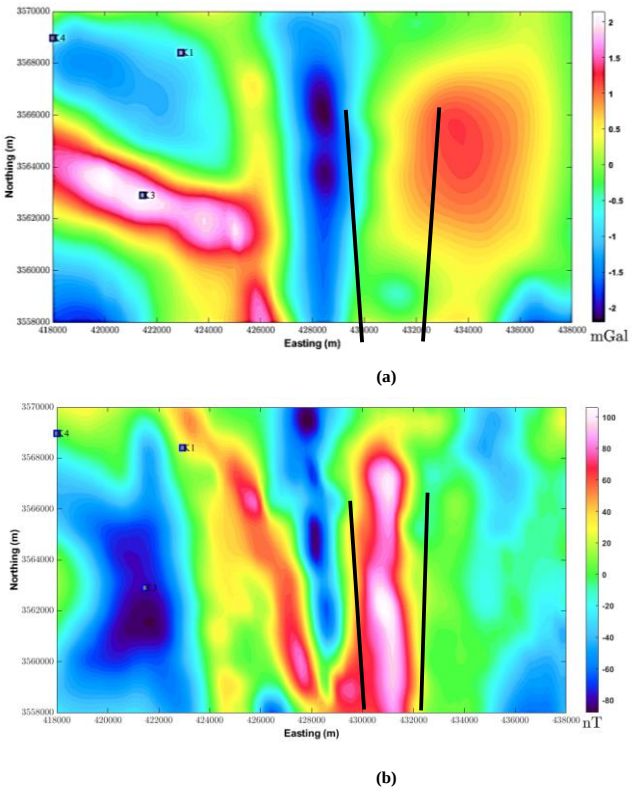

(a)

(b)

Fig. 11 The potential field maps of the Kifl region in Iraq, (a) gravity, and (b) magnetic data along with the drilled wells in the area. The black lines indicate the possible faults of the area according to the previous studies (AL-Farhan et al. 2022).

Figures 13a- c present the Euler depth estimation solutions over the gravity and magnetic maps along with the joint Euler depth solutions. As can be seen, the joint Euler method has retrieved proper depth solutions over the study area, covering the faults, horst, and graben structures with acceptable sorting and clustering of the depth solution ranges. Expanding throughout the area, it is worth noting that the joint Euler results have covered the shortcomings of the separately conducted depth estimations. Figure 13 illustrates the 3D display of the Euler depth estimation solutions for separating the gravity and magnetic fields along with the joint Euler estimations as well.

As can be inferred from the Figs. 12 to 14, investigating the results indicates that the joint Euler algorithm has yielded a better match with previous studies and models in comparison to the separate depth estimations of the potential fields. Especially, reviewing the 3D illustration of the joint Euler results (Figs. 13c and 14c), it is evident that compared to the separately estimated solutions of Euler equations, the presented joint Euler method was able to retrieve the depth solution points along with the slope of the faults, as well as the depth of the bottom of the first sedimentary layer and the depth of the cap rock layer (over the horst-graben region) with better resolution. Comparing the separately conducted estimations with the joint Euler approach results shows that the joint consideration of the magnetic and gravity fields has yielded smoother solutions with proper clustering and better visualization aspects compared to the separately estimated solutions.

Figure 14 depicts a 2D view of the depth solutions for the gravity and magnetic fields along with the joint Euler results. As can be seen, the gravity depth results have yielded better results than the magnetic solutions in terms of uniformity and distribution, clustering, and sorting. However, the joint Euler results were much more precise leading to better visualization and depiction of the subsurface structures. As a result, in comparison to the separately estimated depth solutions, the slope of the subsurface discontinuities along with the over-layer cap

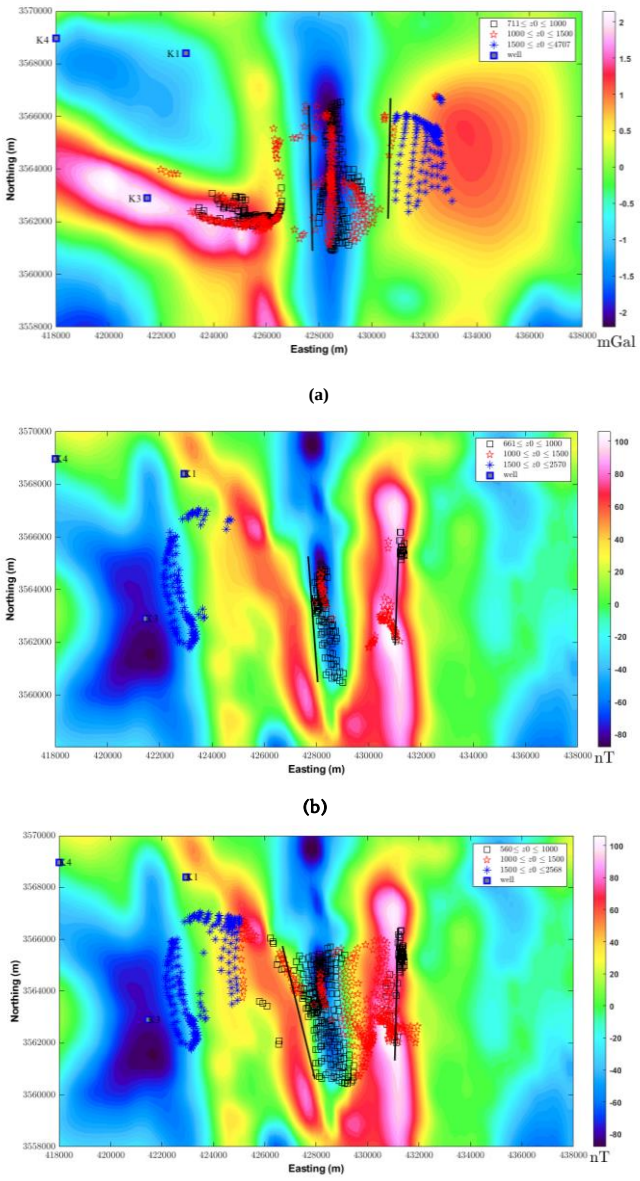

Fig. 12 The standard Euler depth estimation results over an oil-trapping field at the Kifl region in Iraq, (a) gravity estimations, b) magnetic estimations, and (c) joint algorithm estimations superimposed over the magnetic grid.

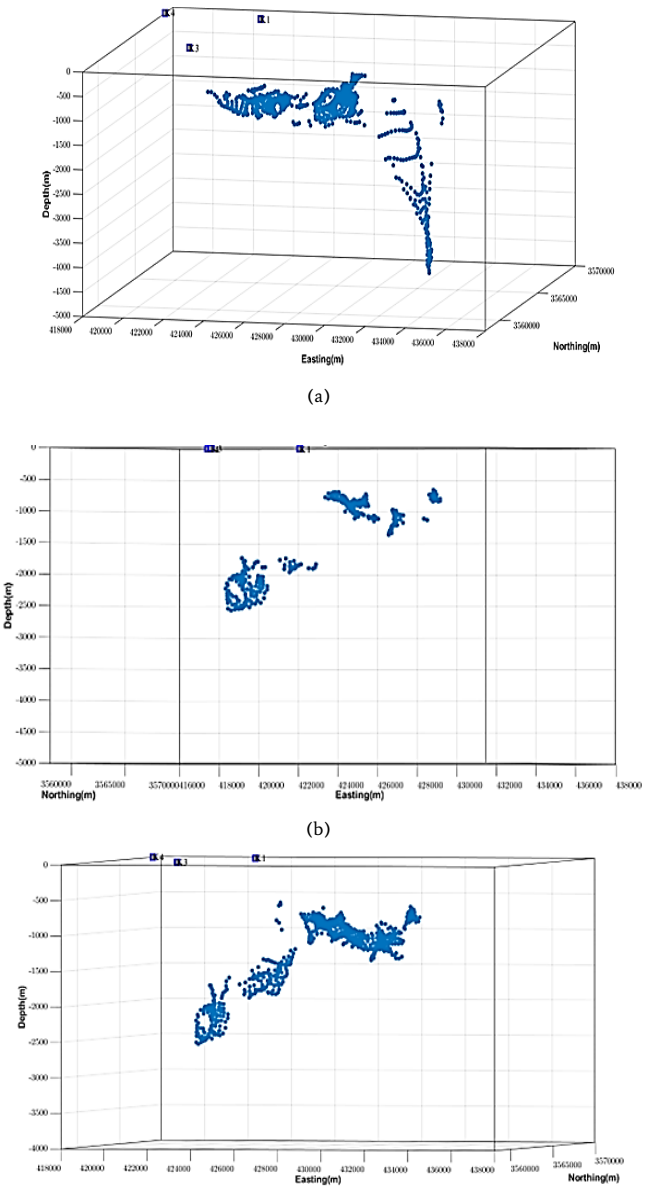

Fig. 13 The 3D visualization of the standard Euler depth estimation results for separate (a) gravity data, (b) magnetic data, and for (c) joint algorithm.

6. Conclusion

The Euler deconvolution technique is a swift and efficient mechanism as a suitable tool in the quantitative and qualitative analysis of potential field data. The low quality and resolution of data caused by environmental factors, such as severe topography or the existence of data deficiency are important and common obstacles in the geophysical potential data processing. As a mathematical idea, the suggested solution to solve this issue is to employ the joint Euler procedure. In a nutshell, in order to dramatically improve the results, this research solved the standard Euler equation for double potential fields for a suitable tolerance, by considering the magnetic and gravity vector fields as a single one. In comparison to the outputs of the separately solved Euler depth estimation equations, the results indicate that combining the characteristics of two different but similar potential vector fields of the magnetic and gravity data help to complete and ameliorate the outcomes of depth estimations over the body and boundary of the potential sources.

To assess the accuracy and precision of the presented method, the joint Euler equations were solved for two homogeneous and non-homogeneous synthetic models, and the results were compared with the separately estimated depth solutions. Within four inconsistent cases, the results of this study specified that the joint Euler method has provided a better quality of estimation results along with more appropriate consistency and sorting of final solutions in addition to a more reliable number of acceptable answers. This proposed method was implemented on an inhomogeneous synthetic model within four various states. Conclusively, the joint Euler method was properly able to yield superior and reliable results for the depth and boundary of the target masses in all four states. As discussed for the fourth case with the non-identical magnetic and gravity field coordinates, along with the increased survey data spacing, separately conducted the Euler depth estimations of the gravity field returned no answers, while the separately acquired solutions for the magnetic data yielded better results. However, through

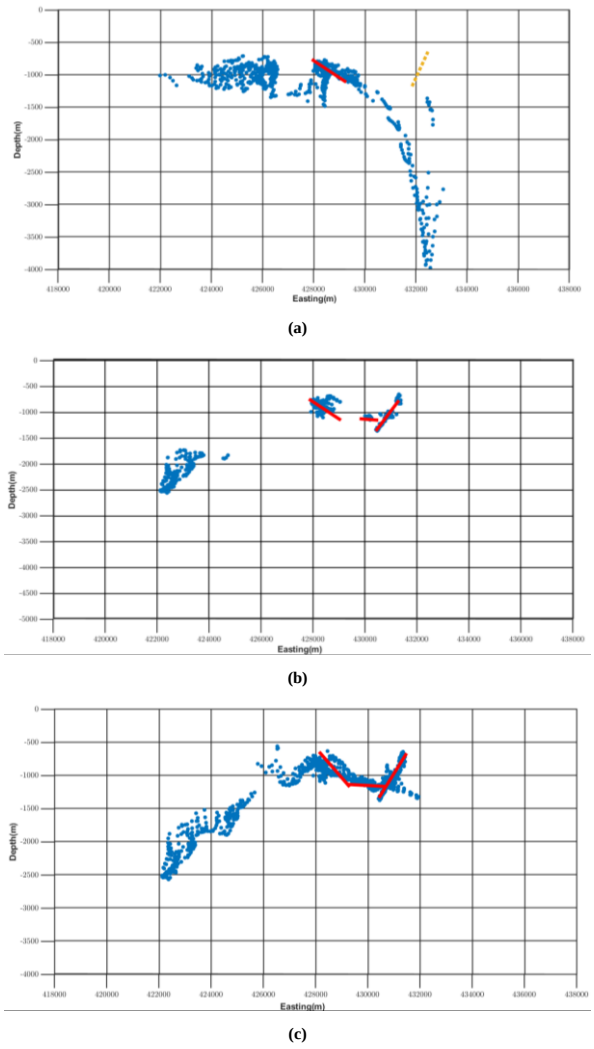

Fig. 14 The 2D visualization of the standard Euler depth estimation results for separate (a) gravity data, (b) magnetic data, and for (c) joint algorithm.

the merger between two mentioned potential fields, the presented joint Euler method in this study was quite able to provide appropriate estimations of the boundary and depth of non-homogeneous targets. Hence, by investigating the synthetic scenarios, rather than separate solutions, it can be concluded that the combination of Euler equations for both magnetic and gravity potential fields results in the desired quality of interest, especially in the low-resolution data sets. Therefore, the novel joint Euler method can be utilized in the interpretations and researches of potential field geophysical data.

After the review and inspection of the favorable conclusions for the designed synthetic models through the low-resolution cases, the proposed method was implemented on the potential field data sets of the Kifl oil reservoir located in Iraq. In comparison with the separate Euler solutions for the potential fields, the results of the joint Euler method returned an acceptable configuration for the subsurface host-graben fault structures along with the depth of the sedimentary overburden cap rock.

Natural density and magnetic susceptibility contrast of rocks are two factors causing potential field anomalies. The mathematical solution concept of the equations proposed in this research were presented and applied by considering the assumption that two types of physical properties of the underground targets and their two resultant potential vector fields can provide more accurate and reliable information together in the quantitative and qualitative interpretational aspects of subsurface structures. As a result, the calculation of Euler equations in joint mode for potential fields can be considered a contemporary and innovative approach within the interpretational point of views in the field of potential field studies.

Acknowledgments

Authors would like to express their sincere thanks to the Institute of Geophysics and the School of Mining Engineering, University of Tehran, for all provided supports.

Funding

The author did not get any funds for doing this study.

Data availability

Data are available on reasonable request to the corresponding author via maysamabedi@ut.ac.ir.

Code availability

The code is developed and maintained by Saeed Ghanbarifar based on MATLAB. Please contact with the corresponding author for code inquiries, accessibility, and required data provision.

Conflict of interest

The authors declare that they have no known competing financial interests or personal relationships that could have appeared to influence the work reported in this paper.

REFERENCES

[1] Thompson DT (1982) EULDPH: A new technique for making computer-assisted depth estimates from magnetic data. Geophysics 47(1): 31-37

[2] Reid AB, Allsop JM, Granser H, Millett AT, Somerton IW (1990). Magnetic interpretation in three dimensions using Euler deconvolution. Geophysics 55(1): 80-91

[3] Okpoli CC (2019) High resolution magnetic field signatures over Akure and its Environs, southwestern Nigeria. Earth Sci Malays 3(1): 9-17

[4] Hosseini SH, Habibian Dehkordi B, Abedi M, Oskooi B (2021) Implications for a Geothermal Reservoir at Abgarm, Mahallat, Iran: Magnetic and Magnetotelluric Signatures. Natural Resources Research 30(1): 259-272

[5] Ghiasi SM, Hosseini SH, Afshar A, Abedi M (2022) A Novel Magnetic Interpretational Perspective on Charmaleh Iron Deposit Through Improved Edge Detection Techniques and 3D Inversion Approaches. Natural Resources Research, 1-24

[6] Reid AB, Thurston JB (2014) The structural index in gravity and magnetic interpretation: Errors, uses, and abuses. Geophysics 79(4): J61-J66

[7] Reid AB, Ebbing J, Webb SJ (2014) Avoidable Euler errors–the use and abuse of Euler deconvolution applied to potential fields. Geophysical Prospecting 62(5): 1162-1168

[8] Ghanbarifar S, Hosseini SH, Abedi M, Afshar A 2023 A dynamic window-based Euler depth estimator for 2 potential field geophysical data. Bulletin of Geophysics and Oceanography, (Accepted for publication).

[9] AL-Farhan M, Oskooi B, Abedi M, Ebrahim Zadeh Ardestani V,

AL-Khalidy A (2022) Implications on oil trapping in the Kifl field of Iraq through geophysical investigations. International Journal of Mining and Geo-Engineering: 56(4), 391-400

[10] AL-Farhan M, Oskooi B, Ebrahim Zadeh Ardestani V, Abedi M, AL-Khalidy A (2019) Magnetic and gravity signatures of the Kifl oil field in Iraq. Journal of Petroleum Science and Engineering: 183, 106397

[11] Abedi M (2022) Cooperative fuzzy-guided focused inversion for unstructured mesh modeling of potential field geophysics, a case study for imaging an oil-trapping structure. Acta Geophysica 70(5): 2077-2098

[12] Fedi M, Florio G, Paoletti V (2015) MHODE: a local-homogeneity theory for improved source-parameter estimation of potential fields. Geophysical Journal International 202(2): 887-900

[13] Barbosa VC, Silva JB, Medeiros WE (1999) Stability analysis and improvement of structural index estimation in Euler deconvolution. Geophysics 64(1): 48-60

[14] Salem A, Ravat D (2003) A combined analytic signal and Euler method (AN-EUL) for automatic interpretation of magnetic data. Geophysics 68(6): 1952-1961

[15] Gerovska D, Araúzo-Bravo MJ (2003) Automatic interpretation of magnetic data based on Euler deconvolution with unprescribed structural index. Computers & Geosciences 29(8): 949-960

[16] Melo FF, Barbosa VC (2018) Correct structural index in Euler deconvolution via base-level estimates. Geophysics 83(6): J87-J98

[17] Aster RC, Borchers B, Thurber C (2018) Parameter estimation and inverse problems. Academic Press, New York, NY.

[18] Chen T. Zhang G (2018) Forward modeling of gravity anomalies based on cell mergence and parallel computing. Computers & Geosciences 120: 1-9

[19] Barbosa VC, Silva JB (2005) Deconvolução de Euler: passado, presente e futuro-um tutorial. Revista Brasileira de Geofísica 23(3): 243-250

[20] Sissakian VK (2013) Geological evolution of the Iraqi Mesopotamia Foredeep, inner platform and near surroundings of the Arabian Plate. Journal of Asian Earth Sciences 72: 152-163

[21] Abdulnaby W (2018) Structural Geology and Neotectonics of Iraq, Northwest Zagros. In book: Tectonic and Structural Framework of the Zagros Fold-Thrust Belt, 10.1016/B978-0-12-815048-1.00004-4.

[22] Sissakian VK, Mohammed BS (2007) Geology of Iraqi Western Desert. Iraqi Bull. Geol. Min. Special Issue: 51-124

[23] Fouad SFA (2010) Tectonic and structural evolution of the Mesopotamia foredeep, Iraq. Iraqi Bulletin of Geology and Mining 6: 41–53

[24] Jassim SZ, Goff JC (2006) Geology of Iraq, Czech Republic, ISBN 80-7028-287-8, pp 341. Prague, 35-52

[25] Al-Banna A (1992) Gravity lineaments, fault trends and depth of the basement rocks in Western Desert. Iraqi J. Sci., 33: 63–79

[26] Hijab BR, Aldabbas MA (2000). Tectonic evolution of Iraq. Iraqi Geological Journal 32: 26-47